LETTER

Fabrication of single phase 2D homologous perovskite microplates by mechanical exfoliation

2D Materials

RECEIVED
8 November 2017

REVISED
4 January 2018

ACCEPTED FOR PUBLICATION
8 January 2018

PUBLISHED
19 January 2018

LETTER

Fabrication of single phase 2D homologous perovskite microplates by mechanical exfoliation

Junze Li[1], Jun Wang[1], Yingjun Zhang[2], Haizhen Wang[3], Gaoming Lin[1], Xuan Xiong[1], Weihang Zhou[2], Hongmei Luo[3] and Dehui Li[1,4]

[1] School of Optical and Electronic Information, Huazhong University of Science and Technology, Wuhan 430074, People's Republic of China
[2] Wuhan National High Magnetic Field Center, Huazhong University of Science and Technology, Wuhan 430074, People's Republic of China
[3] Department of Chemical and Materials Engineering, New Mexico State University, Las Cruces, NM 88003, United States of America
[4] Wuhan National Laboratory for Optoelectronics, Huazhong University of Science and Technology, Wuhan 430074, People's Republic of China

E-mail: dehuili@hust.edu.cn

Keywords: 2D homologous perovskite, pure single phase, mechanical exfoliation, photodetection

Abstract

The two-dimensional (2D) Ruddlesden–Popper type perovskites have attracted intensive interest for their great environmental stability and various potential optoelectronic applications. Fundamental understanding of the photophysical and electronic properties of the 2D perovskites with pure single phase is essential for improving the performance of the optoelectronic devices and designing devices with new architectures. Investigating the optical and electronic properties of these materials with pure single phase is required to obtain pure single phase 2D perovskites. Here, we report on an alternative approach to fabricate $(C_4H_9NH_3)_2(CH_3NH_3)_{n-1}Pb_nI_{3n+1}$ microplates with pure single n-number perovskite phase for $n > 2$ by mechanical exfoliation. Micro-photoluminescence and absorption spectroscopy studies reveal that the as-synthesized 2D perovskite plates for $n > 2$ are comprised by dominant n-number phase and small inclusions of hybrid perovskite phases with different n values, which is supported by excitation power dependent photoluminescence. By mechanical exfoliation method, 2D perovskite microplates with the thickness of around 20 nm are obtained, which surprisingly have single n-number perovskite phase for $n = 2$–5. In addition, we have demonstrated that the exfoliated 2D perovskite microplates can be integrated with other 2D layered materials such as boron nitride, and are able to be transferred to prefabricated electrodes for photodetections. Our studies not only provide a strategy to prepare 2D perovskites with a single n-number perovskite phase allowing us to extract the basic optical and electronic parameters of pure phase perovskites, but also demonstrate the possibility to integrate the 2D perovskites with other 2D layered materials to extend the device's functionalities.

Introduction

Three-dimensional (3D) organic–inorganic lead halide perovskites have attracted extensive attention recently, mainly due to the rapid rise of the power conversion efficiency of perovskite solar cells to more than 22% within just a few years [1–6]. Taking advantages of strong light absorption, modest charge mobility [7], long carrier diffusion length of the 3D perovskite materials [8–10], the perovskite-based transistors [11], photodetectors [12–14], lasers [15, 16] and light-emitting devices [4, 17–21] have been demonstrated. Despite the rapid developments of perovskite-based optoelectronic applications, some drawbacks of 3D perovskites, including the current–voltage hysteresis, long-term stability and toxicity of lead, have to be addressed for commercialization of perovskite-based optoelectronic applications [22–25].

One solution to the long-term stability of 3D perovskites is the two-dimensional (2D) Ruddlesden–Popper perovskites, which have great environmental stability compared with their 3D analogues and thus have attracted increasing interests recently [26–33]. 2D perovskites are defined by a general formula $R_2A_{n-1}Pb_nX_{3n+1}$, where R is long chain spacer cation, A is organic cation, X is a halide anion, n is an integer from

1 to ∞ and represents the number of $[PbX_6]^{4-}$ octahedral sheets sandwiched between two layers of R spacer cations [34]. 2D perovskites can be regarded as two long organic chains R inserting into their bulk perovskites with n indicating the number of $[PbX_6]^{4-}$ octahedral sheets in each unit. The organic chain serves as dielectric layer, thus forming quantum-well structures with remarkable quantum confinement effect and large exciton binding energy [28, 29]. With such a unique structure, they show great environmental stability, remarkable quantum confinement effect and layered characteristic. By changing the chemical composites and n values, their band gap can be readily tuned from near infrared to violet wavelength range and thus might find promising applications in solar cells, photodetectors and light emitting devices with fairly well long-term stability [26, 28, 29, 36–41].

Fundamental understanding of the photophysical and electronic properties of the 2D perovskites with pure single phase is essential for improving the performance of the optoelectronic devices and designing devices with new architectures [42–45]. Here, we provide a mechanical way to obtain pure single phase of 2D perovskites. We fabricate $(C_4H_9NH_3)_2(CH_3NH_3)_{n-1}Pb_nI_{3n+1}$ microplates with different thickness and investigate the photoluminescence (PL) evolution with the thickness. Our micro-PL studies reveal that the as-synthesized 2D perovskite plates with $n > 2$ always contain the small inclusions with different n values even if the molar ratio of the precursors is intended for a single n-number phase. By adopting mechanical exfoliation method, we are able to obtain 2D perovskite microplates with a single n-number perovskite phase when the thickness of the microplates is down to around 20 nm for $n = 3$–5. Finally, we demonstrate that the exfoliated pure phase perovskite microplates can be integrated with boron nitride flakes forming van de Waals (vdW) heterostructure and can be transferred to predefined electrodes functioning as photodetectors.

Methods

Synthesis of perovskite

Methylammonium chloride (MACl) was synthesized by neutralizing a 40% w/w aqueous methylamine (MA) and a 32% w/w aqueous hydrochloric acid (HCl) with a molar ratio of 1:1 with stirring for 2 h at 0 °C. The solvent was then evaporated at 60 °C and washed by diethyl ether three times followed by dried at 70 °C for 12 h. For synthesis of n-butylammonium iodide (BAI) solution, the same procedure was used except that the methylamine was replaced by n-butylamine (BA) and the stirring time was extended to 4 h. For synthesis of $(C_4H_9NH_3)_2(CH_3NH_3)_{n-1}PbnI_{3n+1}$ ($n = 1$–5), PbO powder (0.5 g) was dissolved in a mixture of 57% w/w aqueous hydriodic acid (HI) solution (3 ml) and 50% w/w aqueous hypophosphorous acid (H_3PO_2) solution (0.5 ml) by heating to 140 °C under constant magnetic stirring. Then 2.5 mmol BAI solution was added into the resultant solution for the synthesis of $(BA)_2PbI_4$ plates while a mixture solution of (1.25 mmol; 1.67 mmol; 1.86 mmol; 2 mmol) MACl and (1.75 mmol; 0.83 mmol; 0.62 mmol; 0.5 mmol) BAI were successively injected to the resultant solution for the synthesis of $(C_4H_9NH_3)_2(CH_3NH_3)_{n-1}Pb_nI_{3n+1}$ ($n = 2$–5) plates. Afterwards, the stirring was stopped, and the solution was left to naturally cool to room temperature. The precipitation was left to stand overnight for the growth to be completed.

Device fabrication

For fabrication of hBN/perovskite heterostructure, the perovskite microplates with thickness of 20 nm were peeled off from the as-synthesis $n = 3$ perovskite plates by using Scotch-tape micromechanical cleavage technique onto 300 nm SiO_2 on Si wafer. A thin hBN flake was exfoliated onto a layer of polymethyl methacrylate (PMMA) on Si wafer pretreated by hexamethyldisiloxane (HMDS). Then the PMMA layer is peeled off from silicon substrate and attached to a polydimethylsiloxane (PDMS) stamp with hBN side up. Subsequently, the PDMS stamp with hBN sitting on PMMA film is positioned on a prepared perovskite flakes under the aid of optical microscope and micromanipulators. The substrate was then heated to about 140 °C to release PMMA layer from PDMS stamp. For the fabrication of two-probe devices, 10 nm Cr/100 nm Au electrodes were defined by photolithography and deposited by electron beam evaporation. Then $n = 3$ perovskite flake was exfoliated on PDMS and positioned on the predefined electrodes under the aid of optical microscope and micromanipulator.

Characteristics

Ultraviolet–vis absorbance spectra were performed on a CRAIC 20 micro-spectra photometer with an aperture size of 10 μm. The PL measurements were carried out on Renishaw inVia-Reflex with a 1800 g mm^{-1} grating excited by a 532 nm solid-state laser or a 325 nm He–Cd laser. X-ray diffraction spectra were performed by Bruker D2 PHPSER (Cu Kα $\lambda = 0.154\,19$ nm, Nickel filter, 25 kV, 40 mA). Thickness of the exfoliated microplates was confirmed by atom force microscope (Bruker Dimension Edge). Optical images were acquired by an optical microscope (Mshot-MJ30). The output (I–V) curves were measured in a home-built probe station coupled with a Keithley 2400.

Results and discussion

Figure 1(a) displays schematic illustrations of the crystal structures of $(C_4H_9NH_3)_2(CH_3NH_3)_{n-1}Pb_nI_{3n+1}$ (n is from 1 to 5). 2D perovskites are composed of n layers of $[MX_6]^{4-}$ octahedral sheets sandwiched by two layers of insulating spacers, which are coupled via

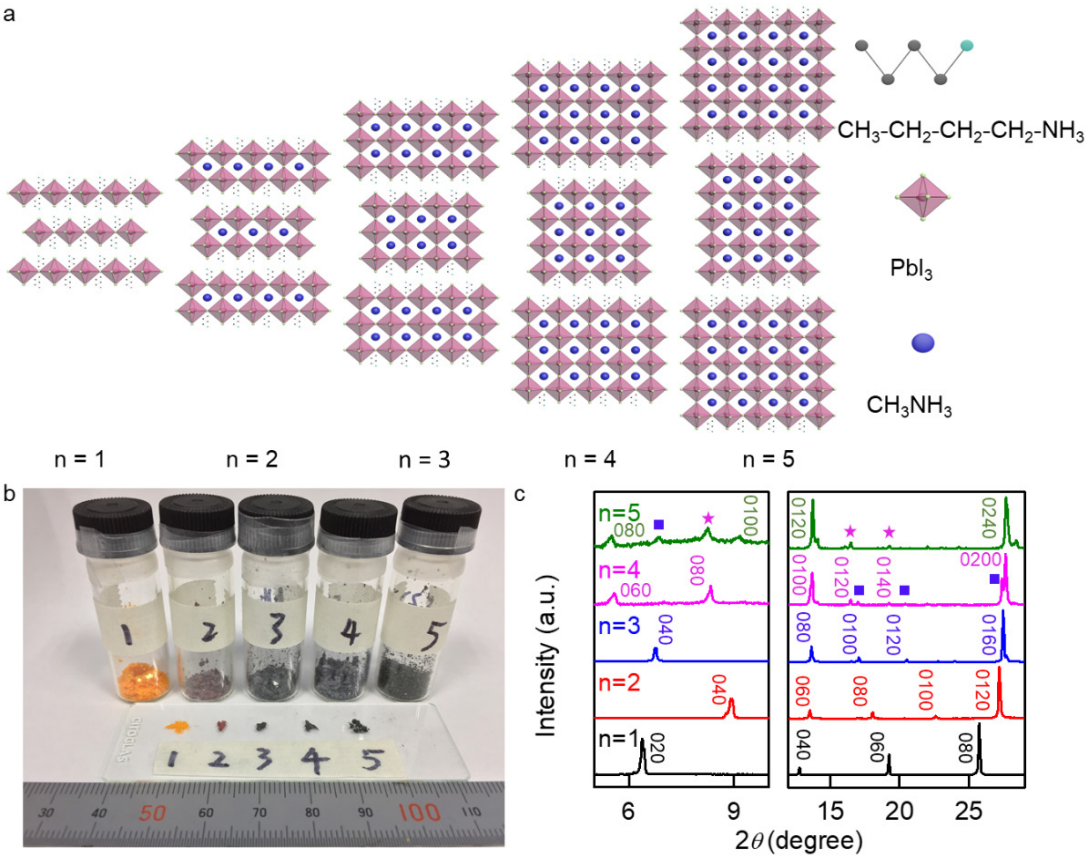

Figure 1. (a) The schematic illustration of crystal structure of $(C_4H_9NH_3)_2(CH_3NH_3)_{n-1}Pb_nI_{3n+1}$ for $n = 1$–5. (b) Photograph of the as-synthesized 2D perovskite plates with $n = 1$–5. The bottom panel displays the single crystal plate for $n = 1$–5 with the size on the order of centimeter. (c) XRD patterns of the as-synthesized 2D perovskite plates for $n = 1$–5 with main peaks indexed. The intensity under 10° has been magnified. Blue square: $n = 3$ perovskite phase within $n = 4$ and $n = 5$ perovskite plates; pink stars: $n = 4$ perovskite phase within $n = 5$ perovskite plates.

vdW interaction. The weak vdW interaction allows us to fabricate thin 2D perovskite plates through mechanical exfoliation method, similar to graphene and 2D transition metal dichalcogenide (TMD) crystals. By adopting solution synthesis method [29,46], we successfully obtained 2D perovskite crystals with centimeter size for $n = 1$–5 by tuning the molar ratio of the precursors (figure 1(b)). The color of as-synthesized 2D perovskite plates changes from yellow to red and finally to dark with the increase of $n = 1$–5 indicating the spectral evolution of the 2D perovskites with the n-number. Powder x-ray diffraction (XRD) patterns suggest that the as-synthesized 2D perovskite plates are possibly pure single n-number perovskite phase for $n = 1$ and 2 while hybrid perovskite phase with different n values is observed for $n = 3$–5, similar to the 2D perovskite films reported (figure 1(c)) [28, 29, 46, 47]. For $n = 4$ 2D perovskite plates, as there are always diffraction peaks from $n = 3$ indicated by blue squares while diffraction peaks from both $n = 3$ and $n = 4$ are present in $n = 5$ 2D perovskite plates indicated by blue squares and pink stars. Even though the molar ratio of the precursors used is intentionally tuned in a large range to synthesize pure single n-number phase perovskites for $n = 4$ and 5, perovskite phases with different n number always coexist.

To investigate the uniformity of the as-synthesized 2D perovskite plates and how the inclusions of the different n-number phases distribute, we carried out micro-absorption measurement with the aperture size of 10 μm at several different locations of the crystals (figures 2(a)–(f)). The band edge of the absorption spectra gradually shifts from 520 nm to around 690 nm with the increase of the n-value due to the quantum confinement effect [35, 46]. For $n = 1$ and $n = 2$ 2D perovskites, the band edge of the absorption spectra shows a very narrow distribution, indicating the pure single phase of $n = 1$ and $n = 2$ 2D perovskites, consistent with results of XRD in figure 1(c). Nevertheless, for $n = 3$–5 2D perovskite plates, the distribution range of absorption edges increases with the increase of the n value (660 nm–680 nm for $n = 3$; 640 nm–690 nm for $n = 4$ and 640 nm–700 nm for $n = 5$), suggesting the mixture of different n-number perovskite phases with n ranging from 3 to ∞ [46]. In addition, compared with the absorption spectra of $n = 1$ and $n = 2$ perovskite plates, the absorption edges are less steep for $n = 3$–5 perovskites, revealing the mixture of the as-synthesized $n = 3$–5 perovskites. The wider distribution of the absorption edge for $n = 3$–5 perovskites acquired at different locations suggests that the coexistence of hybrid phase perovskites distributes

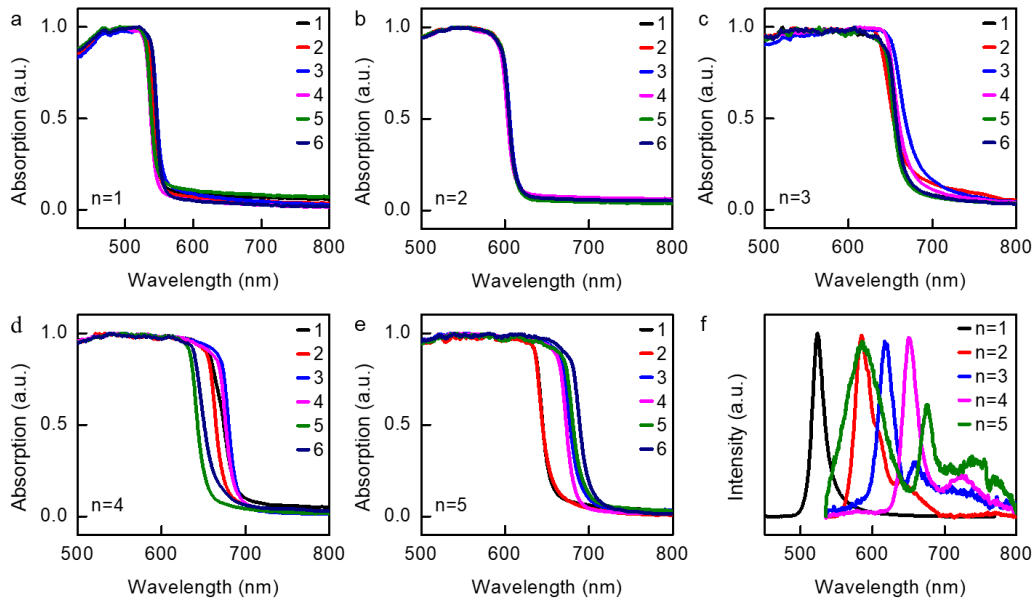

Figure 2. (a)–(e) Absorption spectra of the as-synthesized $(C_4H_9NH_3)_2(CH_3NH_3)_{n-1}Pb_nI_{3n+1}$ plates with n from 1 to 5. For each n-number perovskite plates, absorption spectra are acquired at six different positions to check the uniformity of the samples. The aperture used for absorption measurement is 10 μm. (f) Normalized PL spectra of the as-synthesized $(C_4H_9NH_3)_2(CH_3NH_3)_{n-1}Pb_nI_{3n+1}$ plates for $n = 1$–5. For $n = 3$–5 perovskite plates, multiple emission peaks are observed.

along both lateral and vertical directions within the entire 2D perovskite plates.

We also confirm the coexistence and uniformity of hybrid phase perovskites in the as-grown 2D perovskites by micro-photoluminescence spectroscopy. For each plate of $n = 1$–5 2D perovskites, we acquired several PL spectra from different locations. For $n = 1$ and 2 2D perovskites, only one emission peak appears locating at 520 nm for $n = 1$ and 590 nm for $n = 2$ (figure 2(f)), which coincide with the absorption edge in figures 2(a) and (b) and can be assigned to the free exciton emission according to previous reports [46, 47]. Nevertheless, multiple emission peaks are observed for $n = 3$–5 2D perovskite plates with the emission peak corresponding to $n = 2$–5 or ∞, indicating the presence of the hybrid phase perovskites with different n values. In addition, the PL intensity of $n = 3$–5 2D perovskites greatly decreases likely due to the type-II band alignment of different n-number phases (figure 3(a)). The type-II band alignment would result in that the photogenerated electrons and holes are spatially separated and thus the greatly reduced emission intensity [48].

As discussed above, for the as-synthesized $n = 3$ 2D perovskite plates, all diffraction peaks can be indexed to pure $n = 3$ perovskite phase (figure 1(c)) and absorption spectra show a narrow distribution of absorption edges (figure 2(c)). Therefore, we anticipate the as-synthesized $n = 3$ perovskite plates are relatively pure with small inclusions of different n-number perovskite phases. To confirm this, we carried out the excitation power dependence of PL spectra for $n = 3$ perovskite plates. Under the low power excitation (0.5 μW), two emission peaks are present locating at 620 nm and 650 nm, corresponding to the free exciton emission of $n = 3$ and $n = 4$ perovskite phase, respectively (figure 3(b)). Increasing the excitation power to around 2 μW, the emission peak of $n = 4$ perovskite phase shows a slight blueshift while emission peak of $n = 3$ perovskite phase maintains at the same position compared with that under lower power excitation of 0.5 μW. Nevertheless, compared with the emission intensity from $n = 3$ perovskite phase, the relatively emission intensity of $n = 4$ perovskite phase decreases with the increase of the excitation power. Further increasing the excitation power to 4 μW, the emission from $n = 4$ perovskite phase completely disappears. Both the blueshift of the emission peak and decrease of the relative emission intensity of $n = 4$ perovskite phase with the increase of the excitation power suggest that the dominant phase in the as-synthesized $n = 3$ perovskite plates is $n = 3$ perovskite phase with small inclusions of the $n = 4$ perovskite phase. The inclusions of the $n = 4$ perovskite phase is embedded within the $n = 3$ perovskite phase with very small size such that the band filling effect occurs under excitation resulting in the blueshift of emission peak and saturation of the emission intensity of $n = 4$ perovskite phase with the increase of the excitation power [49, 50].

The presence of band filling effect here rather than the energy funneling effect induced emission enhancement [37] is due to the extremely small size of the $n = 4$ inclusions. From the energy band alignment between $n = 3$ and $n = 4$ phase perovskites (figure 3(a)), the photogenerated carries prefer to occupy the small $n = 4$ inclusions embedded in the $n = 3$ flakes. As the excitation power increases, due to the smaller density of states of those small $n = 4$ inclusions the quasi-Fermi levels of the photogenerated carriers move into

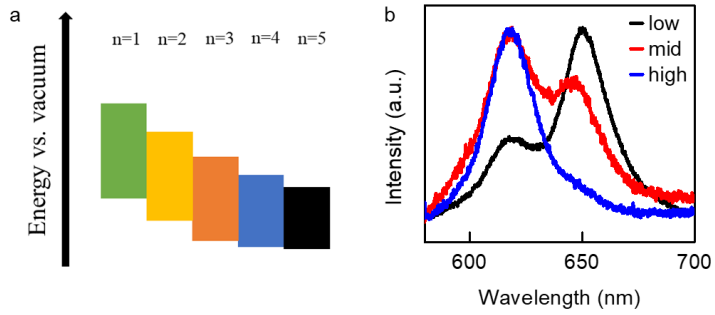

Figure 3. (a) Comparative band energy alignment of $(C_4H_9NH_3)_2(CH_3NH_3)_{n-1}Pb_nI_{3n+1}$ with $n = 1$–5. (b) Normalized PL spectra of the as-synthesized 2D perovskite plates with $n = 3$ phase under different excitation power from 0.5 μW to 4 μW.

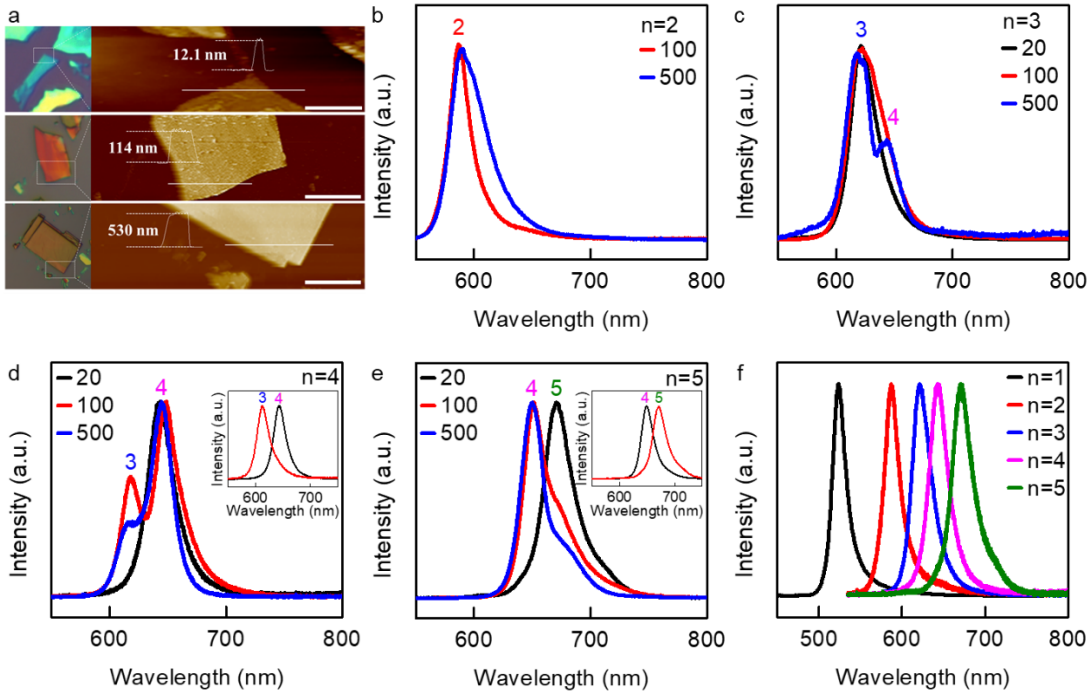

Figure 4. (a) Optical and AFM images of the exfoliated $n = 3$ 2D perovskite microplates with different thicknesses. Scale bars are 2 μm, 4 μm, and 10 μm from top to bottom. (b)–(e) Normalized PL spectra of the exfoliated microplates with different thickness from $n = 1$–5. Insert of (d) and (e) are the normalized PL spectra measured from the different microplates exfoliated from the same $n = 4$ (d) and $n = 5$ (e) 2D perovskite plates. The excitation source is a 532 nm solid-state laser with a power of 0.14 μW. (f) Normalized PL spectra of $n = 1$ perovskite plate and the exfoliated $n = 2$–5 microplate with thickness below 20 nm. For all spectra of $n = 1$–5, only one emission was observed, indicating the pure phase of the exfoliated thin microplates. For $n > 1$, the excitation source is a 532 nm solid-state laser with a power of 0.14 μW while a 325 nm He–Cd laser with a power of 1 μW for $n = 1$.

the conduction band and valence band of $n = 4$ inclusions, resulting in the large blueshift of $n = 4$ emission peak and the saturation of $n = 4$ emission intensity which are the evidences of the band filling effect [51–53]. Thus, we use a very low excitation power of 0.1 μW in the following to avoid the band filling effect and to check whether the as-synthesized 2D perovskites are pure single n-number phase.

The weak vdW interaction between the $[MX_6]^{4-}$ octahedral sheets and organic spacer layers allows us to obtain single n-number phase perovskite via mechanical exfoliation. Figure 4(a) displays the optical images and corresponding atomic force microscope (AFM) images of $n = 3$ perovskite microplates with various thicknesses mechanically peeled by scotch tape. Similar to graphene and 2D TMD crystals, the color of the peeled microplates strongly depends on their thicknesses, which provides a powerful method to identify the thickness of microplates [54]. As seen from figure 4(a), the color changes from yellow to red and finally to green when the thickness decreases from 500 nm to around 20 nm. Similarly, we obtain the microplates with the similar thickness by peeling $n = 2$, 4, and 5 perovskite crystals for further PL studies.

Figures 4(b)–(e) show the PL spectra of exfoliated microplates with different thicknesses for n from 2 to 5. For $n = 1$, we do not expect the presence of the mixed perovskite phases and thus we do not include the PL data from the exfoliated $n = 1$ microplates. Only one emission peak is present for $n = 2$ no matter what the thickness of the exfoliated microplates is.

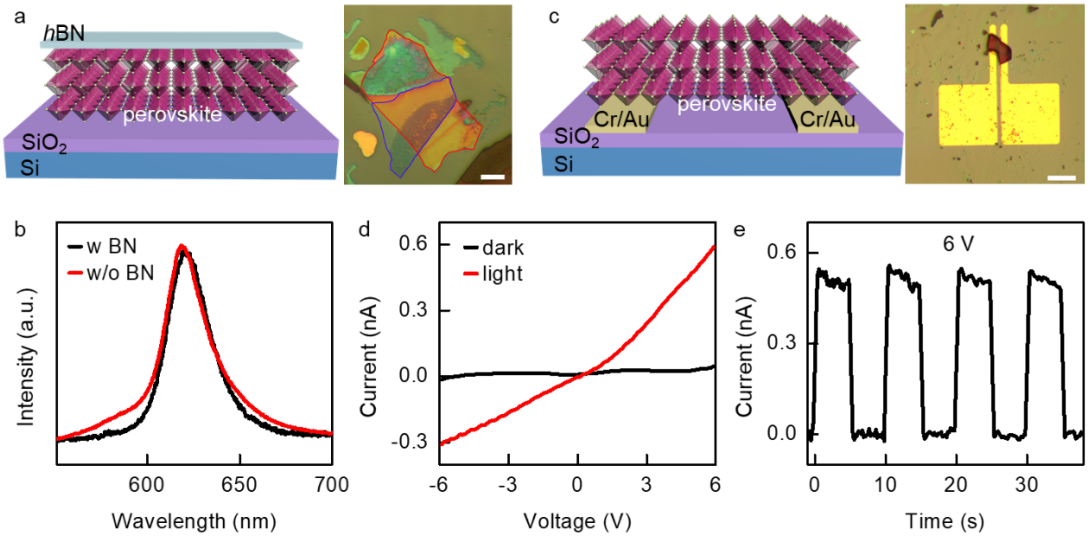

Figure 5. (a) Schematic and optical image of *h*BN/perovskite heterostructure. The *h*BN and perovskite microplates are outlined by red line and blue line, respectively. The scale bar is 10 μm. (b) Normalized PL spectra of the exfoliated microplates under h-BN (black) and without *h*BN (red). (c) Schematic and optical image of the two-probe device. The perovskite microplate was exfoliated from $n = 3$ perovskite plates with a thickness of around 20 nm. The scale bar is 50 μm. (d) The current–voltage curve of the two-probe device in dark and under illumination with a 528 nm LED with a power density of 30 μW cm^{-2}. (e) The optical switching characteristic of the two-probe device illuminated by a 528 nm LED with a power density of 30 μW cm^{-2} under a source-drain voltage of 6 V. The incident light was modulated by a mechanical shutter with a period of 5 s.

In contrast, we always observe two emission peaks for $n = 3$–5 perovskite microplates with thickness larger than 20 nm (microplates with yellow and red color) and one emission peak for those $n = 3$–5 perovskite microplates with thickness below 20 nm (green color microplates). The emission peak of all green microplates exfoliated from $n = 3$ perovskite plates locates at 620 nm (corresponding to the emission peak of $n = 3$ 2D perovskites), which indicates the relative purity of the as-synthesized $n = 3$ perovskite plates, consistent with the results of XRD (figure 1(c)) and absorption measurement (figure 2(c)). Nevertheless, as seen from inset of figures 4(d) and (e) the emission peaks of green microplates exfoliated from $n = 4$ (5) perovskite plates belong to emission peak of $n = 3$ (4) and $n = 4$ (5) perovskite phase, suggesting a large percentage of perovskites with $n = 3$ (4) perovskite phase in the as-synthesized $n = 4$ (5) perovskite plates consistent with results of XRD (figure 1(c)) and absorption spectra (figures 2(d) and (e)). Finally, 2D perovskites with single *n*-number phase from $n = 1$ to $n = 5$ have been successfully prepared with a single emission peak for those flakes with thickness below 20 nm by mechanically exfoliating the corresponding bulk crystals (figure 4(f)), which provide a platform to extract the basic optical and charge transport parameters of pure phase 2D perovskites for further improving the performance of 2D perovskite based optoelectronic devices. The possible reason for such observation is that the perovskites with different *n*-number phase are physically mixed and the mixture is not uniform. Thus, the perovskites with different *n*-number phase exist as isolated blocks with single *n*-number phase perovskites. As a result, by reducing the thickness of the perovskite via exfoliation method, the exfoliated flakes might be solely from the isolated pure phase perovskites and thus the flakes with single-*n* phase are able to be obtained with thickness below 20 nm.

We further demonstrate that the exfoliated single *n*-number 2D perovskite flakes can be integrated with other 2D layered materials such graphene and TMDs [55]. Figure 5(a) shows the schematic and optical images of an exfoliated $n = 3$ perovskite flake with thickness around 20 nm covered by a layer of boron nitride (*h*BN) using alignment transfer technique [56], where the perovskite flake and *h*BN are outlined by blue and red line, respectively. Compared with the PL spectrum of the perovskite flake before covering *h*BN, the emission peak maintains at the same position while the profile of the PL spectrum slight changes at the higher energy side after transferring the *h*BN, which might be due to the reduction of the surface states during the transfer processes (figure 5(b)). This indicates that it is feasible to couple the 2D perovskite with other 2D materials to form complex heterostructures such that the properties of the materials can be greatly extended and designed according to the demanding.

Finally, we adopted the alignment transfer technique to transfer an exfoliated $n = 3$ perovskite microplate with thickness of 20 nm to prefabricated electrodes for photodetection as a demonstration. Figure 5(c) displays the schematic and optical images of the two-probe devices on a 300 nm SiO_2/Si substrate with a channel length of 10 μm. There is no detectable dark current (figure 5(d)), indicating the lack of intrinsic charge carriers (electrons, holes) due to the high crystalline quality of the exfoliated flakes with few defects

(dopants). The asymmetric current–voltage curve shows that the contact is not optimal. Upon illumination (528 nm LED with a power density of 30 μW cm^{-2}), the current rapidly increases to 0.6 nA at a source-drain voltage of 6 V, which corresponds to the photoresponsivity of around 10 A W^{-1}. The optical switching characteristic at 6 V shows the photocurrent changes rapidly with the light on and off, with an on–off ratio of 150 (figure 5(e)). Compared with the graphene-contacted 2D $(C_4H_9NH_3)_2PbBr_4$ perovskite crystal photodetectors reported [36], both photoresponsivity and on–off ratio of our devices are smaller, which might be due to the poor contact and small thickness of the exfoliated microplates we used. With further optimization of contact, we expect that the performance of our photodetectors can be greatly improved.

Conclusion

In conclusion, we have prepared single *n*-number phase 2D perovskites of $n = 1$–5 for the first time by mechanical exfoliation. Our XRD, PL and absorption studies indicate that the as-synthesized 2D perovskite plates for $n = 3$–5 always comprise hybrid perovskite phases with different *n* values, which prevents us to extract basic optical and charge transport parameters of the single *n*-number phase perovskites. By adopting the mechanical exfoliation method, we successfully obtained 2D perovskite microplates with thickness below 20 nm, which are proved to be single *n*-number perovskite phases via PL measurement. Finally, we successfully integrated the exfoliated single *n*-number phase perovskite microplate with 2D *h*BN flakes and fabricated the two-probe photodetectors. Our findings develop one method to prepare single *n*-number phase perovskite microplates and thus offer a platform to investigate the basic optical and electronic properties of pure phase 2D perovskites, which can provide valuable information for improving the performance of optoelectronic devices and designing new device architectures.

Acknowledgments

DL acknowledges the support from NSFC (61674060) and the Fundamental Research Funds for the Central Universities, HUST (2017KFYXJJ030, 2017KFXKJC003, 2017KFXKJC002) and National Young 1000 Talent Plan of China; HL thanks the support from New Mexico EPSCoR with NSF-1301346. We thank Hong Cheng engineer in the Analytical and Testing Center of Huazhong University of Science and Technology for the support in PL measurement and thank the Center of Micro-Fabrication of WNLO for the support in device fabrication.

ORCID iDs

Dehui Li https://orcid.org/0000-0002-5945-220X

References

[1] Lee M M *et al* 2012 Efficient hybrid solar cells based on meso-superstructured organometal halide perovskites *Science* **338** 643–7
[2] Green M A, Ho-Baillie A and Snaith H J 2014 The emergence of perovskite solar cells *Nat. Photon.* **8** 506–14
[3] Yang W S *et al* 2015 High-performance photovoltaic perovskite layers fabricated through intramolecular exchange *Science* **348** 1234–7
[4] Xiao Z *et al* 2017 Efficient perovskite light-emitting diodes featuring nanometre-sized crystallites *Nat. Photon.* **11** 108–15
[5] Saliba M *et al* 2016 Incorporation of rubidium cations into perovskite solar cells improves photovoltaic performance *Science* **354** 206–9
[6] Nie W Y *et al* 2015 High-efficiency solution-processed perovskite solar cells with millimeter-scale grains *Science* **347** 522–5
[7] Shi D *et al* 2015 Low trap-state density and long carrier diffusion in organolead trihalide perovskite single crystals *Science* **347** 519–22
[8] Johnston M B and Herz L M 2016 Hybrid perovskites for photovoltaics: charge-carrier recombination, diffusion, and radiative efficiencies *Acc. Chem. Res.* **49** 146–54
[9] Brenner T M *et al* 2016 Hybrid organic–inorganic perovskites: low-cost semiconductors with intriguing charge-transport properties *Nat. Rev. Mater.* **1** 15007
[10] Huang J *et al* 2017 Understanding the physical properties of hybrid perovskites for photovoltaic applications *Nat. Rev. Mater.* **2** 17042
[11] Li D *et al* 2017 The effect of thermal annealing on charge transport in organolead halide perovskite microplate field-effect transistors *Adv. Mater.* **29** 1601959
[12] Li W *et al* 2017 Chemically diverse and multifunctional hybrid organic–inorganic perovskites *Nat. Rev. Mater.* **2** 16099
[13] Wei W *et al* 2017 Monolithic integration of hybrid perovskite single crystals with heterogenous substrate for highly sensitive x-ray imaging *Nat. Photon.* **11** 315–21
[14] Dong Y *et al* 2016 Improving all-inorganic perovskite photodetectors by preferred orientation and plasmonic effect *Small* **12** 5622–32
[15] Xing G C *et al* 2014 Low-temperature solution-processed wavelength-tunable perovskites for lasing *Nat. Mater.* **13** 476–80
[16] Li X *et al* 2017 Amino-mediated anchoring perovskite quantum dots for stable and low-threshold random lasing *Adv. Mater.* **29** 1701185
[17] Wang N *et al* 2016 Perovskite light-emitting diodes based on solution-processed self-organized multiple quantum wells *Nat. Photon.* **10** 699–704
[18] Quan L N *et al* 2017 Tailoring the energy landscape in quasi-2D halide perovskites enables efficient green-light emission *Nano Lett.* **17** 3701–9
[19] Byun J *et al* 2016 Efficient visible quasi-2D perovskite light-emitting diodes *Adv. Mater.* **28** 7515–20
[20] Kim Y H, Cho H and Lee T W 2016 Metal halide perovskite light emitters *Proc. Natl Acad. Sci. USA* **113** 11694–702
[21] Cho H C *et al* 2015 Overcoming the electroluminescence efficiency limitations of perovskite light-emitting diodes *Science* **350** 1222–5
[22] Li X *et al* 2015 Improved performance and stability of perovskite solar cells by crystal crosslinking with alkylphosphonic acid omega-ammonium chlorides *Nat. Chem.* **7** 703–11
[23] Rong Y *et al* 2015 Beyond efficiency: the challenge of stability in mesoscopic perovskite solar cells *Adv. Energy Mater.* **5** 1501066
[24] Wang Z *et al* 2017 Stability of perovskite solar cells: a prospective on the substitution of the A cation and X anion *Angew. Chem., Int. Ed. Engl.* **56** 1190–212
[25] Chiang C H *et al* 2017 The synergistic effect of H_2O and DMF towards stable and 20% efficiency inverted perovskite solar cells *Energy Environ. Sci.* **10** 808–17

[26] Smith I C *et al* 2014 A layered hybrid perovskite solar-cell absorber with enhanced moisture stability *Angew. Chem., Int. Ed. Engl.* **53** 11232–5
[27] Pedesseau L *et al* 2016 Advances and promises of layered halide hybrid perovskite semiconductors *ACS Nano* **10** 9776–86
[28] Cao D H *et al* 2015 2D Homologous perovskites as light-absorbing materials for solar cell applications *J. Am. Chem. Soc.* **137** 7843–50
[29] Stoumpos C C *et al* 2016 Ruddlesden–Popper hybrid lead iodide perovskite 2D homologous semiconductors *Chem. Mater.* **28** 2852–67
[30] Dou L T *et al* 2015 Atomically thin two-dimensional organic–inorganic hybrid perovskites *Science* **349** 1518–21
[31] Tsai H *et al* 2016 High-efficiency two-dimensional Ruddlesden–Popper perovskite solar cells *Nature* **536** 312–6
[32] Dou L 2017 Emerging two-dimensional halide perovskite nanomaterials *J. Mater. Chem.* C **5** 11165–73
[33] Wang J *et al* 2017 Controllable synthesis of two-dimensional Ruddlesden–Popper-type perovskite heterostructures *J. Phys. Chem. Lett.* **8** 6211–9
[34] Song J *et al* 2016 Monolayer and few-layer all-inorganic perovskites as a new family of two-dimensional semiconductors for printable optoelectronic devices *Adv. Mater.* **28** 4861–9
[35] Hong X, Ishihara T and Nurmikko A V 1992 Dielectric confinement effect on excitons in PbI_4-based layered semiconductors *Phys. Rev.* B **45** 6961–4
[36] Tan Z *et al* 2016 Two-dimensional $(C_4H_9NH_3)_2PbBr_4$ perovskite crystals for high-performance photodetector *J. Am. Chem. Soc.* **138** 16612–5
[37] Yuan M J *et al* 2016 Perovskite energy funnels for efficient light-emitting diodes *Nat. Nanotechnol.* **11** 872–7
[38] Ha S T *et al* 2016 Laser cooling of organic–inorganic lead halide perovskites *Nat. Photon.* **10** 115–21
[39] Wang Z *et al* 2017 Efficient ambient-air-stable solar cells with 2D–3D heterostructured butylammonium–caesium–formamidinium lead halide perovskites *Nat. Energy* **6** 17135
[40] Gan X *et al* 2017 2D Homologous organic–inorganic hybrids as light-absorbers for planer and nanorod-based perovskite solar cells *Sol. Energy Mater. Sol. Cells.* **162** 93–102
[41] Yu D *et al* 2017 Dimensionality and interface engineering of 2D homologous perovskites for boosted charge-carrier transport and photodetection performances *J. Phys. Chem. Lett.* **8** 2565–72
[42] Milot R L *et al* 2016 Charge-carrier dynamics in 2D hybrid metal-halide perovskites *Nano Lett.* **16** 7001–7
[43] Guo Z *et al* 2016 Electron–phonon scattering in atomically thin 2D perovskites *ACS Nano* **10** 9992–8
[44] Yu D *et al* 2017 Enhancing optoelectronic properties of low-dimensional halide perovskite via ultrasonic-assisted template refinement *ACS Appl. Mater. Interfaces* **9** 39602–9
[45] Yu D *et al* 2017 Cation exchange-induced dimensionality construction: from monolayered to multilayered 2D single crystal halide perovskites *Adv. Mater. Interfaces* **4** 1700441
[46] Stoumpos C C *et al* 2017 High members of the 2D Ruddlesden–Popper halide perovskites: synthesis, optical properties, and solar cells of $(CH_3(CH_2)_3NH_3)_2(CH_3NH_3)_4Pb_5I_{16}$ *Chemistry* **2** 427–40
[47] Blancon J C *et al* 2017 Extremely efficient internal exciton dissociation through edge states in layered 2D perovskites *Science* **355** 1288–91
[48] Liu J *et al* 2017 Observation of internal photoinduced electron and hole separation in hybrid two-dimentional perovskite films *J. Am. Chem. Soc.* **139** 1432–5
[49] Li D H *et al* 2016 Size-dependent phase transition in methylammonium lead iodide perovskite microplate crystals *Nat. Commun.* **7** 11330
[50] Li D *et al* 2015 Strain-induced spatially indirect exciton recombination in zinc-blende/wurtzite CdS heterostructures *Nano Res.* **8** 3035–44
[51] Liu Q *et al* 1995 Evidence of type-II band alignment at the ordered GaInP to GaAs heterointerface *J. Appl. Phys.* **77** 1154–8
[52] D'Innocenzo V *et al* 2014 Tuning the light emission properties by band gap engineering in hybrid lead halide perovskite *J. Am. Chem. Soc.* **136** 17730–3
[53] Di D *et al* 2015 Size-dependent photon emission from organometal halide perovskite nanocrystals embedded in an organic matrix *J. Phys. Chem. Lett.* **6** 446–50
[54] Blake P *et al* 2007 Making graphene visible *Appl. Phys. Lett.* **91** 063124
[55] Cheng H C *et al* 2016 Van der Waals heterojunction devices based on organohalide perovskites and two-dimensional materials *Nano Lett.* **16** 367–73
[56] Castellanos-Gomez A *et al* 2014 Deterministic transfer of two-dimensional materials by all-dry viscoelastic stamping *2D Mater.* **1** 011002